Petroleum Science 21 (2024) 1780–1795

Contents lists available at ScienceDirect

Petroleum Science

journal homepage: www.keaipublishing.com/en/journals/petroleum-science

Original Paper

Micromechanism and mathematical model of stress sensitivity in tight reservoirs of binary granular medium

Jian-Bang Wu [a, b], Sheng-Lai Yang [a, *], Qiang Li [a], Kun Yang [a], Can Huang [a], Dao-Ping Lv [c], Wei Zhou [c]

[a] State Key Laboratory of Petroleum Resources and Engineering, China University of Petroleum (Beijing), Beijing, 102249, China
[b] Laboratoire de Géologie, Ecole Normale Supérieure/CNRS UMR8538, PSL Research University, Paris, 75005, France
[c] Research Institute of Exploration and Development, Xinjiang Oilfield Company, Karamay, 834000, Xinjiang, China

ARTICLE INFO

Article history:
Received 10 May 2023
Received in revised form
30 October 2023
Accepted 11 January 2024
Available online 12 January 2024

Edited by Meng-Jiao Zhou

Keywords:
Stress sensitivity
Binary granular medium
Tight reservoir
Online-NMR
Reservoir energy retention rate

ABSTRACT

Research on reservoir rock stress sensitivity has traditionally focused on unary granular structures, neglecting the binary nature of real reservoirs, especially tight reservoirs. Understanding the stress-sensitive behavior and mathematical characterization of binary granular media remains a challenging task. In this study, we conducted online-NMR experiments to investigate the permeability and porosity evolution as well as stress-sensitive control mechanisms in tight sandy conglomerate samples. The results revealed stress sensitivity coefficients between 0.042 and 0.098 and permeability damage rates ranging from 65.6% to 90.9%, with an average pore compression coefficient of 0.0168–0.0208 MPa^{-1}. Pore-scale compression occurred in three stages: filling, compression, and compaction, with matrix pores playing a dominant role in pore compression. The stress sensitivity of binary granular media was found to be influenced by the support structure and particle properties. High stress sensitivity was associated with small fine particle size, high fines content, high uniformity coefficient of particle size, high plastic deformation, and low Young's modulus. Matrix-supported samples exhibited a high irreversible permeability damage rate (average = 74.2%) and stress sensitivity coefficients (average = 0.089), with pore spaces more slit-like. In contrast, grain-supported samples showed low stress sensitivity coefficients (average = 0.021) at high stress stages. Based on the experiments, we developed a mathematical model for stress sensitivity in binary granular media, considering binary granular properties and nested interactions using Hertz contact deformation and Poiseuille theory. By describing the change in activity content of fines under stress, we characterized the non-stationary state of compressive deformation in the binary granular structure and classified the reservoir into three categories. The model was applied for production prediction using actual data from the Mahu reservoir in China, showing that the energy retention rates of support-dominated, fill-dominated, and matrix-controlled reservoirs should be higher than 70.1%, 88%, and 90.2%, respectively.

1. Introduction

Porous granular media rocks serve as storage for hydrocarbons and the sequestration of greenhouse gases. Their transport properties and mechanical characteristics hold great practical significance (Chen et al., 2023; Guéguen and Boutéca, 2004; Wang et al., 2023; Zhang et al., 2019). Changes in stress cause deformation of the rock skeleton, influencing its physical properties—a phenomenon known as stress sensitivity of the reservoir. Stress sensitivity is extensively studied in geological energy research (Crawford et al., 2023; Dormieux et al., 2011; Kang et al., 2022; Zhong et al., 2020b). In petroleum development, particularly in tight reservoirs, the granular rocks often consist of a stacking of different particles at various levels. Previous studies focused on single-component particles like clean sandstones may not directly apply to such broadly graded media (Dormieux et al., 2011; Li et al., 2022b; Sayers, 2023; Thevanayagam, 2000). This paper investigates the micro-

* Corresponding author.
E-mail address: yangsl@cup.edu.cn (S.-L. Yang).

https://doi.org/10.1016/j.petsci.2024.01.012

mechanisms and mathematical models of stress sensitivity in binary granular media reservoirs.

Researchers have extensively explored the relationship between confining pressure and rock permeability, primarily through experimental studies. The concept of effective stress, introduced by Terzaghi, laid the groundwork for stress sensitivity research (Han et al., 2022; Terzaghi and Peck, 1948). A series of experiments have shown that the response of particles and pores to stress is crucial factors in controlling stress sensitivity (Bernabé et al., 2003; Fatt and Davis, 1952; Li et al., 2022a; Zhao et al., 2013, 2022). Stress sensitivity and media deformation properties vary significantly in reservoirs with different lithology and sedimentary environments (Liu et al., 2020; Li et al., 2013; Tai and Dong, 2022; Zhang et al., 2016). Many studies have shown that particle deformation and fine particle migration clogging are important mechanisms of stress sensitivity (He et al., 2022; Xiao et al., 2016; Xu et al., 2023; Zhong et al., 2020a). McLatchie et al. studied stress sensitivity due to elastic and plastic deformation using reversible and irreversible permeability (McLatchie et al., 1958), with unrecoverable particle rearrangement being the main cause of plastic deformation (Cao and Lei, 2019). Various empirical formulas, such as exponential and porosity-permeability types, have been studied and summarized by scholars based on experimental understanding (David et al., 1994; Holt et al.; Raghavan and Chin, 2002). While these simplified models are easy to use, they lack microstructural parameters that are essential for understanding rock properties. To conduct more comprehensive studies on the stress sensitivity with theoretical guidance, researchers have used rock particle size composition models to study the evolution of rock permeability and porosity under different effective stresses through mechanical analysis (Digby, 1981; Guéguen and Fortin, 2013; Liu et al., 2020; Tian et al., 2015). However, the common single-particle model led to inconsistent results for rocks with significant lithological differences, thus indicating poor applicability.

Current research on stress-sensitivity based on the particle analysis predominantly relies on the mono-particle hypothesis, which may not fully represent real reservoirs, especially tight reservoirs composed of multiple granular media. Conglomerate, a typical binary structure sedimentary rock, can exhibit different stress sensitivities depending on the support structure, i.e., the composition and distribution relationship of support and filling phases (Núñez-González et al., 2016; Sonmez et al., 2006). Nanoindentation studies by Liu et al. and Shi et al. have shown that the gravel in most conglomerates is over three times harder than the matrix (Liu et al., 2022; Shi et al., 2021). Gao et al. and Zhou et al. have highlighted the significant influence of fine particle properties on the permeability and mechanical properties of binary granular materials like conglomerates (Gao et al., 2023; Zhou et al., 2018). However, quantitative experimental and model characterization of the influence of support structure and particle properties on the stress sensitivity of binary particle structures are lacking, and further research is needed.

The Hertz contact deformation theory is widely used for granular media deformation (Gangi, 1978; Li et al., 2023). Some scholars developed a quantitative stress sensitivity model for tight reservoirs, considering particle size and elasticity (Liu et al., 2020; Cao and Lei, 2019; Zhang et al., 2014). However, this model is limited to single mechanical structure elements where all particles participate in contact deformation. Thevanayagam et al. (2002) and Chang and Yin (2011) proposed a binary granular contact theory based on force chains, highlighting that in binary granular structures, some fine particles may not participate in force transfer. In this case, a suitable simplification method is to view the binary granular medium's structural framework as two nested structures. Analyzing the compression characteristics and interactions of these elements provides an effective approach to understand stress sensitivity in binary particle media.

Conventional methods mainly focus on stress sensitivity at the core scale, overlooking the variation of different scales and types of pores in binary granular media (Tian et al., 2022). To address this limitation, online nuclear magnetic resonance (online-NMR) offers valuable insights by providing T_2 relaxation distributions at different confining pressures, revealing the evolution of pore space at various scales (Zhang et al., 2019, 2023). This allows for a more precise understanding of the causes behind changes in porosity and permeability under different confining pressures. In conclusion, this quantitative analysis of pore behavior is essential for a comprehensive understanding of stress sensitivity in binary granular media.

In this study, we employed X-ray diffraction (XRD) and scanning electron microscopy (SEM) to characterize the particle size and mineral composition of the samples. Online-NMR was utilized to analyze changes in different supported pores under varying effective stress conditions. Based on these findings, we investigated the evolution characteristics and underlying control mechanisms of stress sensitivity in porosity and permeability. Building on this, we proposed a stress-sensitive model for binary granular media combining Hertz contact deformation theory with Poiseuille's law, considering particle size and properties. Furthermore, it incorporated production predictions to provide a basis for numerical simulations.

2. Experimental materials and methods

2.1. Core samples and pretreatment

Natural core samples were drilled from the entire diameter samples of Mahu depression, with a diameter of 2.50 ± 0.03 cm. Six samples were selected for online-NMR experiments with lengths ranging from 5.40 to 6.72 cm, ensuring that the length-to-diameter ratio was greater than 1.5:1. Parallel samples were used for mineralogical experiments. Prior to experimentation, the cores were cleaned with a 75% alcohol and 25% benzene solution to eliminate residual oil and subsequently dried. Helium porosity and gas permeability tests were conducted. Sample details are presented in Table 1.

2.2. Petrological analysis experiments

SEM observations were conducted using a Quanta 200F field emission scanning electron microscope platform. The freshly crushed sample surface was bombarded with an electron beam for direct observation of characteristics like interstitial material, pore structure, and cementation.

The cast thin section (CTS) experiment involved injecting colored liquid into rock pores under vacuum pressure, followed by grinding the rocks into thin slices and examining the reservoir structure under a microscope. Pore structure, mineralogy, and support structure analysis were then performed.

The particle size of the samples was tested using an MS2000 laser particle size analyzer. After taking parallel samples and dispersing them, the particle size distribution ranging from micron to millimeter was analyzed. The mineral composition of the samples was quantitatively analyzed using a D8 Focus X-ray diffractometer in an XRD test.

2.3. Online-NMR based stress sensitivity experiments

Stress sensitivity experiments used ISCO precision displacement pumps and HAS confining pressure pumps. NMR measurements

Table 1
Petrophysical property parameters of the samples.

Label	*D*, mm	*L*, cm	ϕ, %	*k*, mD	Lithofacies	Mineral composition, wt%					Particle mass content[a], wt%			Support structure
						Qtz	Pl	Or	Dol	Clay	Coarse gravel	Fine gravel	Sand, silt	
T1	25.12	6.45	8.93	1.102	Traction flow sandy Conglomerate	67.91	11.43	18.28	1.36	1.02	9.61	48.90	41.49	Grain-supported
T2	24.96	5.95	9.62	1.023		61.53	11.30	25.11	0.51	1.55	10.06	46.77	43.17	
Pc	24.90	6.12	12.1	0.395	Pebbled gritty sandstone	50.51	13.23	30.06	3.61	2.59	14.51	43.52	41.98	
Pf	25.06	6.72	5.32	0.120	Pebbled fine sandstone	48.88	15.88	26.88	1.67	6.69	1.96	30.29	67.75	Matrix-supported
G1	25.10	5.52	4.13	0.050	Gravity flow sandy Conglomerate	41.74	15.88	38.02	0	4.36	27.44	26.63	45.93	
G2	24.97	5.40	4.94	0.058		41.24	15.88	38.53	0	4.35	27.80	26.86	45.34	

[a] In the table: *D* is core diameter; *L* is core length; ϕ is helium porosity; *k* is gas permeability; Qtz is quartz; Pl is plagioclase; Or is orthoclase; Dol is dolomite.

were taken using a SPEC-1 instrument for online dynamic monitoring. Kerosene was used as a saturated liquid to avoid water sensitivity effects. The samples were evacuated and saturated at atmospheric pressure for 24 h, followed by 12 h at 25 MPa to ensure full saturation (Wang et al., 2017; Zhang et al., 2020d). During stress sensitivity experiments, confining pressure was varied while maintaining constant pore pressure. Assuming the effective stress coefficient is 1, changes in confining pressure correspond to effective stress changes. Flow pressure was set at 2 MPa, and confining pressure was gradually increased from 7 MPa, at 5 MPa intervals. Permeability and T_2 spectrum were measured under different effective stresses (5, 10, 15, 20, 25 and 30 MPa) until permeability changes were less than 0.0001 mD. Subsequently, confining pressure was gradually decreased.

For online-NMR measurement, the core holder was double-coated with fluorine oil to change confining pressure. The holder, made of polyether ether ketone, did not interfere with NMR measurements. Main NMR measurement parameters included 64 scans, a waiting time of 5000 ms, 10240 acquisition points, and a pulse interval of 80 us.

The T_2 distribution obtained from low-field NMR is primarily dependent on surface relaxation, which occurs at the interface of the liquid and the pore. Surface relaxation can be expressed as a function of the pore radius r and pore shape factor F_s (Li et al., 2013):

$$\frac{1}{T_2}=\frac{1}{T_{2S}}=\rho\frac{F_s}{r} \tag{1}$$

where T_2 denotes the transverse relaxation; T_{2S} is the surface relaxation; ρ is a constant that represents the relaxation strength. It can be observed that the relaxation time is positively correlated with the pore size. The peak area of the T_2 distribution reflects the pore volume (Gupta et al., 2019). This is the theoretical basis for the analysis of NMR T_2 spectra.

2.4. Methods of data analysis

The relationship between effective stress and permeability/porosity in rocks depends on the rock's microscopic characteristics. Therefore, it's vital to choose an appropriate analysis method. Currently, the most common method is the permeability damage rate (e.g., Eq. (2)). However, it only analyzes stress-sensitive states at the first and last moments, overlooking the process. To improve this, the stress sensitivity coefficient (e.g., Eq. (3)) is used. It utilizes the exponential term coefficients fitted to the experimental data to characterize the overall stress sensitivity (Chen et al., 2015; Ivars et al., 2011) :

$$D=\left(1-\frac{K}{K_0}\right)\times 100\% \tag{2}$$

$$\frac{dK}{K}=-\gamma d\sigma \tag{3}$$

where D is the permeability damage rate corresponding to the pressure; K_0 is the initial permeability, mD; K is the permeability under the corresponding effective stress, mD; σ is the effective stress, MPa; γ is the stress sensitivity coefficient. The greater the stress sensitivity coefficient, the more serious the permeability damage. Based on the NMR principle, the compressibility of porosity can be determined by calculating the envelope area of the T_2 spectrum curve (Li et al., 2013):

$$C_P=-\left(\frac{S_i/S_0-1}{\sigma_i-\sigma_0}\right)_{P_P} \tag{4}$$

where C_P is the pore compressibility coefficient, MPa^{-1}, which represents the compression degree of the pore relative to the original state when the effective stress increases; S_i and σ_i are the T_2 spectrum envelope area and confining pressure under the corresponding effective stress; S_0 and σ_0 are the envelope area and confining pressure under the initial state; P_P implies a constant pore pressure. The larger the pore compressibility coefficient, the stronger the compressibility of the pore volume.

The stress sensitivity of rock permeability is influenced by both the compression and geometric characteristics of the pores. The compression characteristics can be characterized by the pore compressibility coefficient, while the geometric characteristics can be characterized by the pore-permeability power exponent (Faruk, 2000):

$$\frac{K}{K_0}=\left(\frac{\phi}{\phi_0}\right)^{\alpha} \tag{5}$$

where α is the power exponent of porosity-permeability; ϕ/ϕ_0 is the ratio of the porosity at the effective stress to the initial porosity. A smaller α indicates pores that are closer to spheroids, while a larger α signifies pores that resemble slit (Liu et al., 2020).

3. Results

3.1. Grain size and pore size

The Ø value method, proposed by Krumbein in 1934, is a widely used quantitative evaluation technique for the particle size distribution of clastic rocks. It defines $Ø=\log_2 D_p$ (D_p being the particle diameter). Particles with Ø less than −3.3 ($D_p > 10$ mm) are coarse gravel, while those with Ø between −3.3 and −2 (4 mm < D_p < 10 mm) are fine gravel. Sand and silt are particles with Ø greater than −2 ($D_p < 4$ mm). Based on the principle of NMR, larger T_2 values indicate larger pore sizes in tight clastic rocks. Pores can be categorized into matrix micropores (T_2 < 5 ms), granular macropores (5 ms < T_2 < 100 ms), and giant pores-fractures

(T_2 > 100 ms) according to their size (Krumbein, 1934; Mitchell and Soga, 2005; Xiao et al., 2019), as shown in Fig. 1.

Fig. 2 illustrates the pore size distribution and particle size probability curves of six samples. The T series and Pc samples display peak positions at Ø = −2.585 (D_p = 6 mm) and Ø = 0 (D_p = 1 mm), indicating binary structures of fine gravel and coarse sand as the coarse and fine particles. The pore distribution is bimodal, showing slight fine skewness. The Pf sample concentrates its particle diameter distribution at 0 < Ø < 1, with mainly fine sand and silt (0.5–1 mm) and fewer gravel. In contrast, the G series samples exhibit a clear binary distribution with peak positions at Ø = −3 (D_p = 8 mm) and Ø = 1 (D_p = 0.5 mm). These samples are primarily composed of binary structures of medium-coarse gravel and coarse sand as the coarse and fine particles. The pore distribution shows a single matrix pores peak. Moreover, the G series samples have less than 30% content of coarse gravel, which exists without a supporting role in a floating state (Liu et al., 2022; Zhang et al., 2020b).

3.2. Microstructural and depositional environments

The grain and pore size variation in the studied samples relates to microstructural differences due to various depositional environments. The microstructure of the rock significantly affects the stress sensitivity. The depositional environment has a direct effect on the microstructure of rocks (Xu et al., 2018; Zhong et al., 2020b). CTS and XRD experiments reveal mineralogical and microstructural results of samples from different sedimentary rock phases. The samples mainly consist of four lithofacies.

Traction flow sandy conglomerate (T samples) and pebbly coarse sandstones (Pg sample) develop at the bottom and top of fan channels or underwater diversion channels microfacies, respectively. They show normal hydraulic sorting and low clay content (< 2%). Grains are mostly in point contact, and the cementing type is mainly inserted or pore-inserted, with grain-supported as the dominant support mechanism, as shown in Fig. 3(a), (c), and (d). This gives it a potentially better mechanical stability (Zhou et al., 2018). Pebbly fine sandstones (Pf sample) mainly occur at the far sand bar, beach bar interbedding, and locally observed in braided channels. They have high clay content (> 6%), with a small amount of floating gravel among the fine sand. The cementing type is basal cementation, and the support structure is matrix support. Gravity flow sandy conglomerates (G samples) develop in debris flow and clastic flow microfacies, characterized by low porosity (< 5%) and low permeability (< 0.1 mD). The cementation type is basal or porous cementation, and the support structure is matrix-supported, as shown in Fig. 3(b), (e), and (f). This type of structure may be more susceptible to stress changes (Chen et al., 2022). Notably, individual coarse gravels with D_p > 16 mm are present, but the content of fine gravels is low, and gravel intervals are filled with mud under weak hydrodynamic environments. The resulting pore space is dominated by matrix pores with dense physical properties. (Yang et al., 2022; Zhang et al., 2020a, 2020c).

3.3. Permeability stress sensitivity

Based on the experimental results in Fig. 4(a) and Eq. (2), the stress-sensitive permeability damage rate *Dm* is obtained when *K* is taken to the permeability under the effective stress of 30 MPa. Irrecoverable damage rate *Ds* is obtained when *K* is taken to the permeability under the effective stress recover to 5 MPa. According to Fig. 4(b) and Eq. (3), the stress sensitivity coefficient (γ) of the rock was obtained as the exponential coefficient item of the formula obtained after integrating Eq. (3). The results show that the sandy conglomerate had a stress-sensitive permeability damage rate of 65.6%–90.9%, an irrecoverable damage rate of 46.9%–80.5%, and a stress sensitivity coefficient of 0.042–0.093. Based on these results, the test cores were divided into two groups: Group A with the stress sensitivity coefficient of 0.042–0.049, consisting of T series and Pc samples, which generally had lower permeability stress sensitivity than Group B with the stress sensitivity coefficient of 0.086–0.093, consisting of Pf and G series samples.

3.4. Pore volume compressibility

According to the NMR relaxation spectrum and Eq. (3), the pore volume compressibility decreases with increasing confining pressure, indicating weaker pore compressibility, as shown in Fig. 5(a). This is due to the increased contact of hard coarse grains, which leads to particles shifting from main structural to main body deformation, reducing the plugging effect of fine particle rearrangement on large pores (Gao et al., 2019). The average pore volume compressibility ranges from 0.0168 to 0.0208 MPa^{-1}. Group A samples (0.0168–0.0177 MPa^{-1}) show weaker compressibility than Group B samples (0.0185–0.0208 MPa^{-1}) due to the protective effect of more coarse-grain contact on fine particle deformation. Further discussion on the support structure's influence will follow.

3.5. Power exponent of porosity-permeability

Porosity and permeability under different effective stress were used to draw a porosity-permeability double-logarithmic curve using Eq. (5), as shown in Fig. 5(b). Curve fitting revealed the porosity-permeability exponent for the tight sandy conglomerate samples ranged from 3.33 to 5.50, with a fitting correlation coefficient greater than 0.99. Group A samples had a porosity-

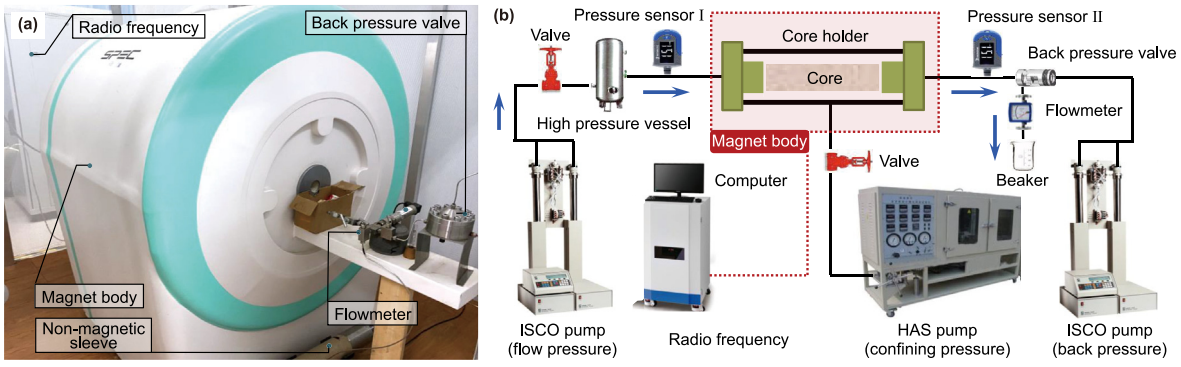

Fig. 1. **(a)** Physical map of NMR equipment. **(b)** Flowchart of the online-NMR-based stress-sensitive test setup.

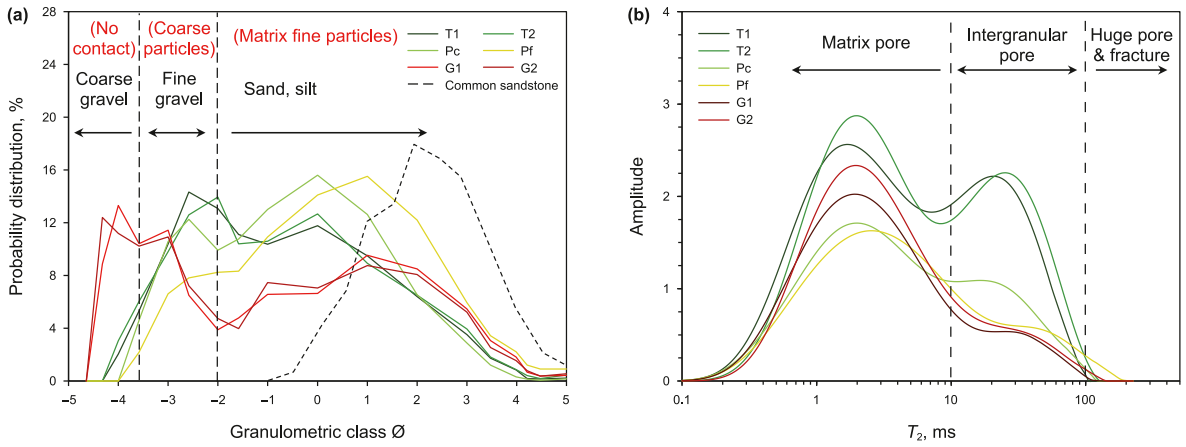

Fig. 2. **(a)** Granularity distribution and **(b)** pore size distribution for the six samples.

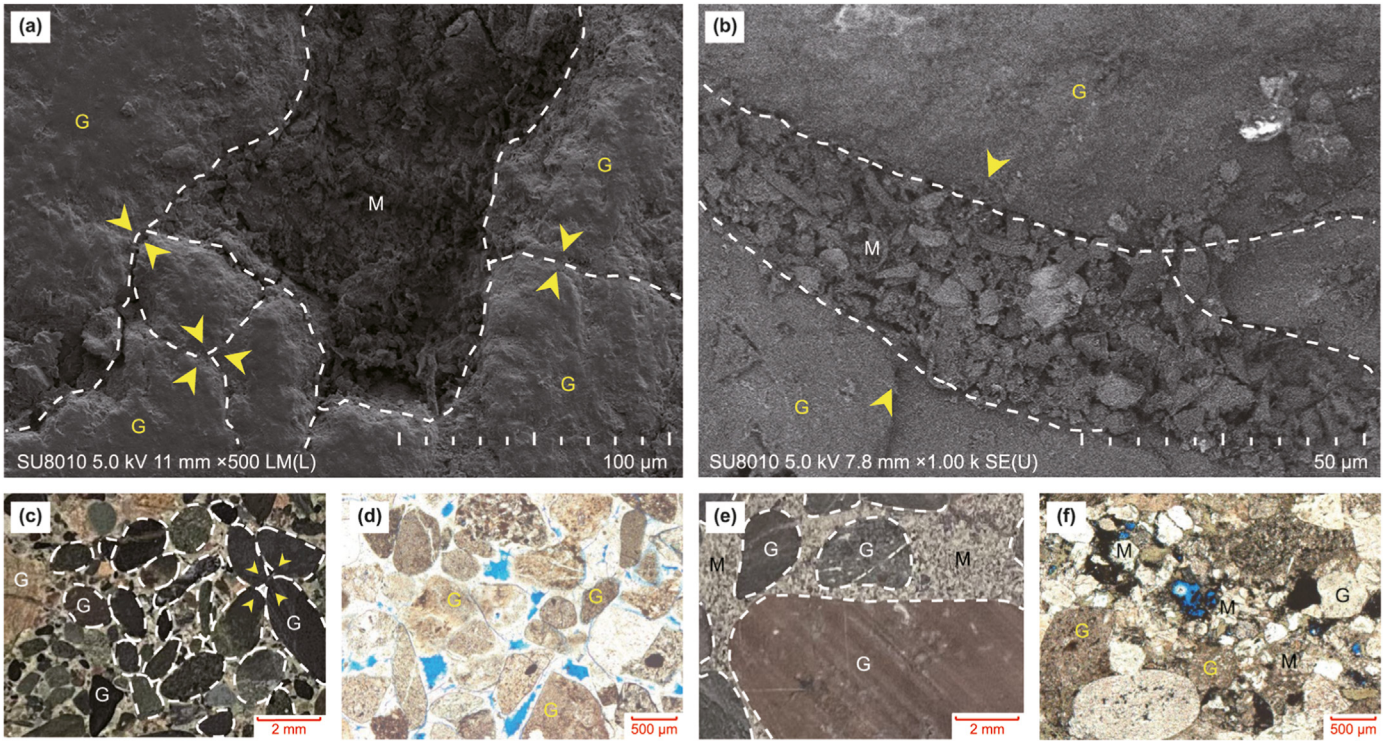

Fig. 3. Microscopic images of sandy conglomerate samples. SEM and CTS photographs of grain-supported samples are shown in **(a)**, **(c)**, and **(d)**, respectively. Most of the visible particles are in direct point contact or line contact. **(b)**, **(e)**, and **(f)** are photographs of matrix-supported samples. The particles are filled with different diameter detrital complex. G refers to hard coarse particles; M refers to the matrix between the particles; the dotted line is the edge of the particles; the arrow is the direction of grains compression when stress is applied.

permeability exponent ranging from 3.33 to 4.19, lower than Group B samples (4.47–5.50). Fractures are more likely to be compressed under effective stress, which leads to a sharp change in permeability. A larger porosity-permeability exponent indicates that the decrease in pore volume is caused more by changes in fracture porosity, which is more sensitive to changes in permeability, and that fracture-like pores are more developed (Liu et al., 2020). This suggests Group A retained more spherical pores after compression, while Group B produced more slit-like pores (Petunin et al., 2011).

4. Discussion

4.1. Evolution of pore space—effect of pore type

Based on NMR experiments, the compression of sandy conglomerate can be classified into three distinct stages by comparing the stage compression rates of micropores and macropores. Set the stage pore compression ratio E_p for a given scale pore as

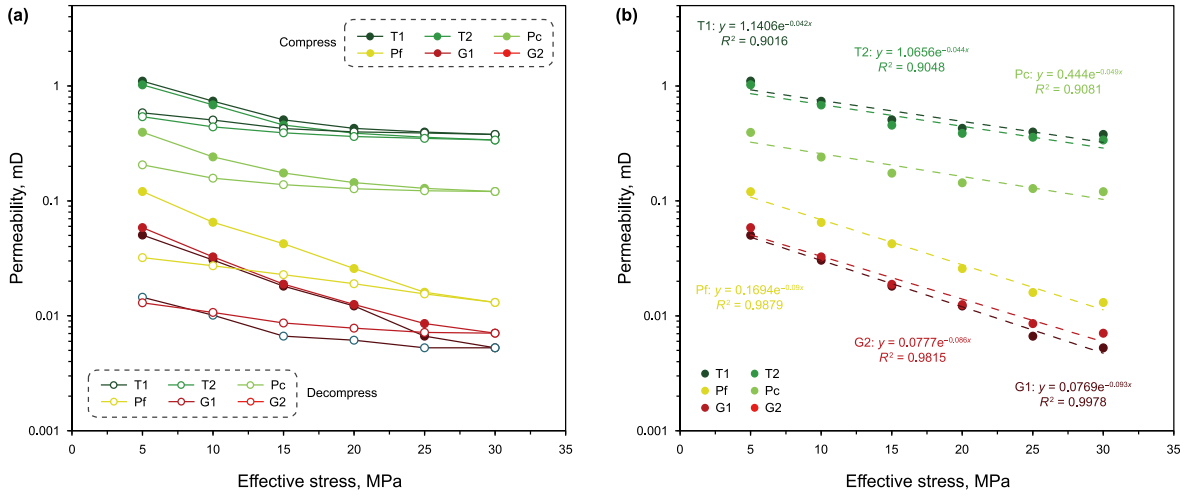

Fig. 4. **(a)** Variation of the permeability of the samples with effective stress during pressurisation and depressurisation. **(b)** Stress sensitivity coefficients were obtained by exponential fitting (exponential term coefficients) of the permeability and effective stress of the compression process.

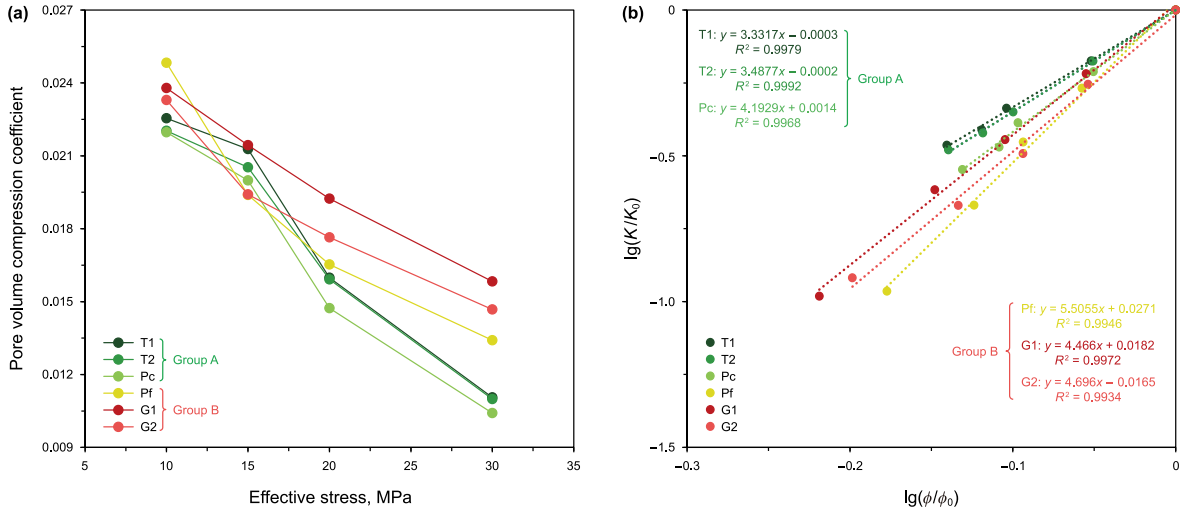

Fig. 5. **(a)** Pore volume compressibility and **(b)** pore permeability exponent for the six samples.

$$E_p(i) = \frac{S_{i-1} - S_i}{\Delta S_{total}} \tag{6}$$

where S_i and S_{i-1} are the T_2 spectral areas at a given pressure and the previous pressure, respectively; ΔS_{total} is the sum of the reduced T_2 spectral areas throughout the pressurisation process. Set the following comparison coefficient ζ as the basis for classifying the compression stage:

$$\zeta(i) = \log_2\left(\left(E_p(i)\right)_{macropore} \Big/ \left(E_p(i)\right)_{micropore} \right) \tag{7}$$

The compression stages, as shown in Fig. 6(a)–(c), can be classified based on Eq. (7). The first stage, known as the filling stage, occurs at the onset of effective stress increase. In this stage, $\zeta(i) > 1$, the stage compression rate of macropores is more than 2 times that of micropores. This is explained by the filling of matrix particles resulting in a significant reduction in macropore volume, whereas the change in micropores is negligible. The second stage, referred to as the compression stage, occurs when the effective stress reaches 2–3 times the initial stress, and $1 > \zeta(i) > -1$. During this stage, both macropore and micropore volumes decrease considerably due to structural deformation of particles, leading to a substantial decline in permeability. The third stage, termed the compaction stage, takes place as the effective stress continues to increase. At this point $\zeta(i) < -1$, the stage compression rate of the micropores is more than 2 times that of the macropores. Since the bulk deformation of the particles primarily occurs at this stage, the pore compaction is dominated by micropores compaction rather than macropores between the hard coarse grains, leading to a comparatively smaller decrease in total pore volume and a slower reduction in permeability.

In Fig. 6(d), the compression coefficients of granular macropores initially show high values but then decrease, while the compression coefficients of matrix micropores start with low values and then increase. This trend aligns with the filling, compression, and compaction process. The average compression coefficients for micropores in T1, Pc, Pf, and G1 cores were 0.0146, 0.0053, 0.0168, and 0.0207 MPa^{-1}, respectively. For macropores, the values were 0.0270, 0.0156, 0.0547, and 0.0564 MPa^{-1}. Micropores' compressibility is closer to the overall pore compressibility, indicating that the pore compression is mainly controlled by matrix pores. The

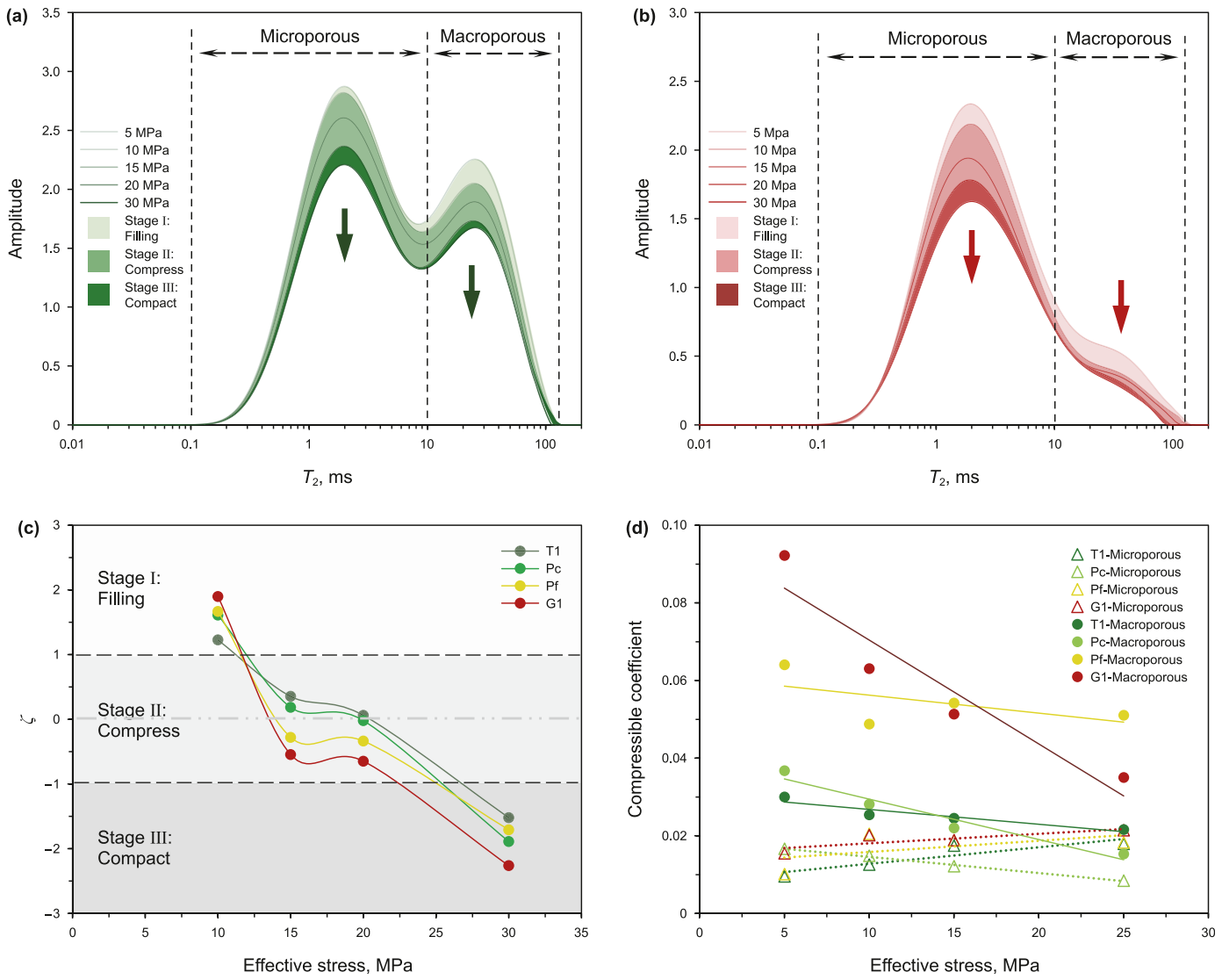

Fig. 6. **(a)** and **(b)** are NMR transverse relaxation spectra of representative samples of grain-supported (T1) and matrix-supported samples (G1) during the increase in effective stress. **(c)** is the variation with pressure of the comparison coefficients of stage compression ratio for macropores and micropores. **(d)** is pore volume compression coefficients for the effective stress increase process for large and small pores for both samples.

macropore compression coefficients in matrix-supported samples Pf and G1 are significantly higher due to limited space for filling within fewer intergranular macropores. Conversely, less coarse-grain support leads to a stronger reduction of pore space through filling and structural deformation of finer particles.

4.2. Evolution of permeability—difference of support structure

Experimental results reveal two types of sandy conglomerate with binary granular media: matrix support (Group B) and particle support (Group A) (Cheng et al., 2023; Liu et al., 2022; Thevanayagam et al., 2002). Significant differences are observed in permeability damage rate, stage stress sensitivity, and irreversible permeability damage rate between the two support structures.

Firstly, concerning permeability damage rate, Group B's matrix-supported samples exhibit ineffective support by hard particles, with the heterogeneous matrix mainly controlling percolation channels. This results in low initial permeability and high permeability damage rate (Figs. 3 and 4). On the other hand, Group A's grain-supported samples benefit from interactions between hard particles, absorbing part of the effective stress, resulting in higher initial permeability and weaker permeability damage.

Secondly, in terms of stage stress sensitivity, stress sensitivity coefficients in the first and second stages for matrix-supported samples exceed 0.06, while grain-supported samples have stress sensitivity coefficients in the second stage all less than 0.03, as shown in Fig. 7(a). This difference arises from the ability of hard particles in the later stage to bear a significant portion of the stress, making it challenging for seepage channels to further close without rupture, as shown in Fig. 8. Compared to matrix-supported samples experiencing sustained matrix compression, grain-supported samples display a stable second stage of permeability stress sensitivity.

Lastly, regarding irreversible permeability damage rate, matrix-supported samples show a high degree of irreversible damage (> 70%), as shown in Fig. 7(b). This is attributed to plastic deformation of the matrix, leading to significant hysteresis in permeability reverting. Conversely, grain-supported samples

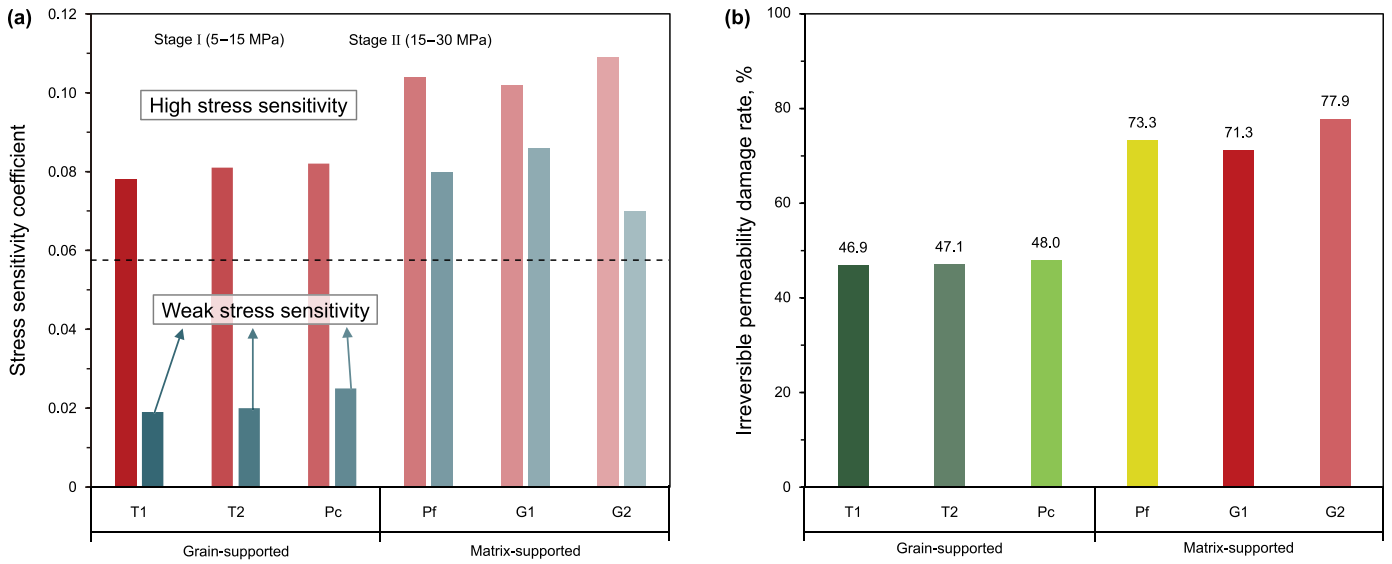

Fig. 7. Stress sensitivity coefficient at different stages and irreversible permeability damage rate. **(a)** is the stress sensitivity factor for six samples at two stages before and after an effective stress of 15 MPa. **(b)** is the irreversible stress-sensitive damage rate for the six samples.

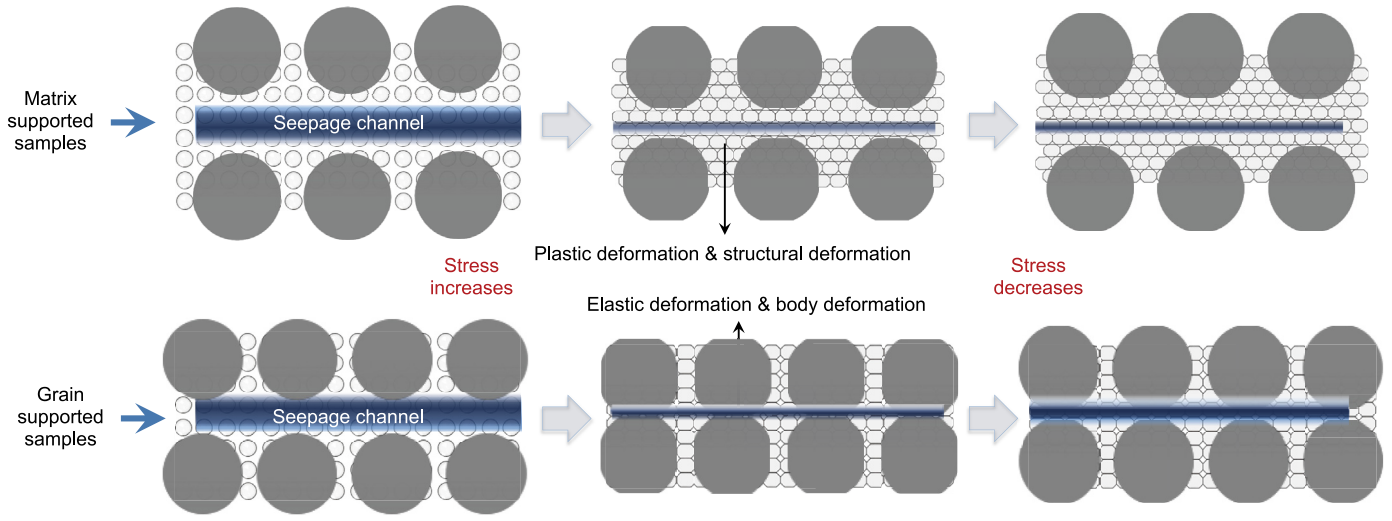

Fig. 8. Schematic representation of the evolution of the seepage channel during the process of particle compression and revert. The top section displays a matrix-supported sample, where the matrix particles are directly compressed and undergo structural and plastic deformation with high levels of irreversible damage. On the other hand, the bottom section shows a grain-supported sample, where elastic deformation and body deformation occur in contact with hard particles, leading to low levels of irreversible damage.

exhibit a low degree of irreversible damage (< 50%) due to elastic deformation of hard particles like quartz after compression, resulting in a better reversion of percolation channels.

4.3. Stress sensitivity coefficients—influence of particle features

Particle features are direct and vital factors in understanding the physical property evolution of binary granular media under different stress conditions (Cheng et al., 2023; Liu et al., 2020; Zhou et al., 2018). However, the correlation between particle size and stress-sensitive damage lacks consensus (Gu et al., 2018; Liu et al., 2020). Relying solely on average particle size is inadequate for accurately measuring stress-sensitive damage. This study found that particle features such as fines content, uniformity coefficient, Young's modulus, and deformation properties, exert significant effects on stress sensitivity.

The duality of particle structure of samples renders average particle size unreliable for evaluating stress sensitivity ($R^2 < 0.3$), as shown in Fig. 9(a). In weakly stress-sensitive Group A samples with grain-supported structure, fine gravels or coarse sands dominate, resulting in an average grain size of 2–4 mm. In strongly stress-sensitive Group B samples with matrix-supported structure, Pf samples have an average particle size less than 2 mm due to high fine sands content, while G series samples are larger than 4 mm due to individual coarse gravel presence. But the seepage channel is still controlled by the shaly matrix formed by debris flow deposition and subsequent reconstruction. In contrast, the average size of fines (sand and silt with $\emptyset > -2$) shows a better negative correlation ($R^2 > 0.8$) with stress sensitivity coefficient. Smaller fines are easier to transport and fill into pores between coarse grains during compression, leading to seepage channel blockage and permeability reduction (Chang et al., 2017a; Yang et al., 2022).

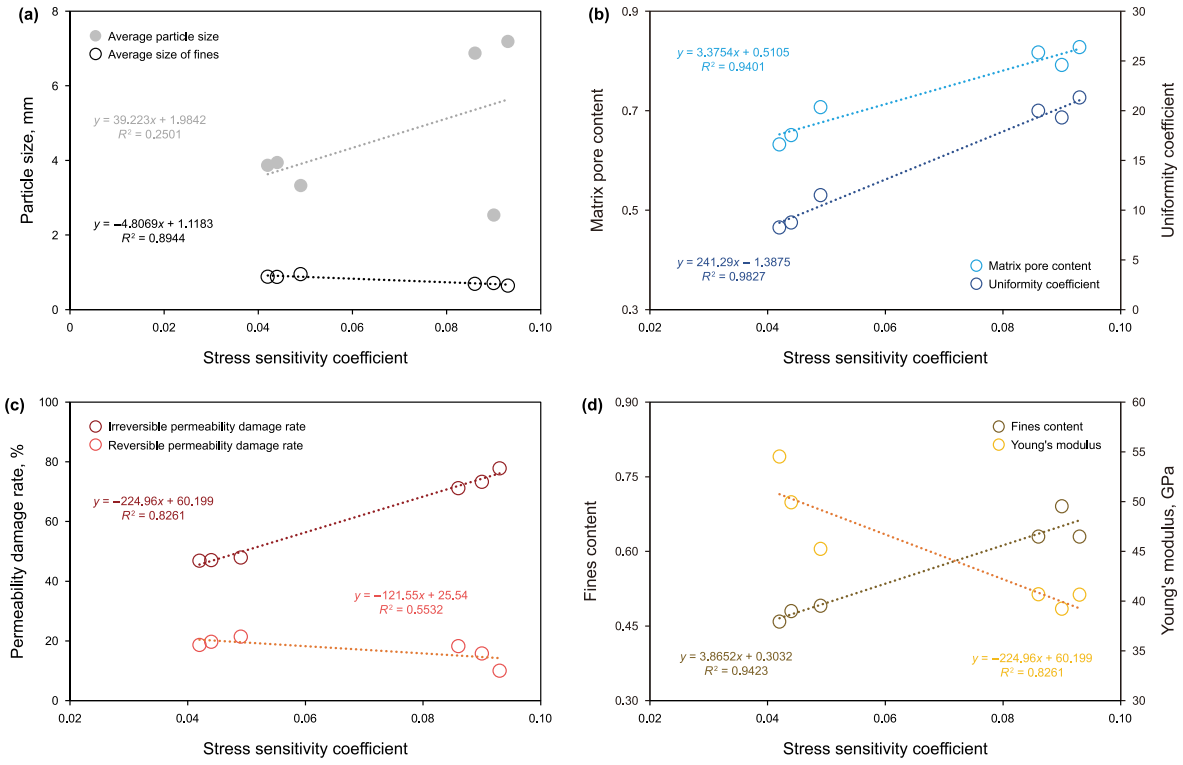

Fig. 9. Stress sensitivity coefficients versus rock structure parameters: **(a)** Average particle size and fines average particle size; **(b)** Uniformity coefficient and matrix pore content; **(c)** Irreversible and reversible permeability damage rates; **(d)** Fines content and Young's modulus.

The uniformity coefficient (C_u) of particle size, matrix pore content, and stress sensitivity coefficient shows a strong positive correlation ($R^2 > 0.9$), as shown in Fig. 9(b). C_u is defined as the ratio of D_{60} to D_{10}, indicating the difference between coarse and fine particle sizes in the sample (Monkul et al., 2021). D_{60} and D_{10} are the diameter of the cumulative accounts for 60% and 10% (Bell, 2013). The matrix pore content is the ratio of the T_2 spectral area of the matrix pores to the total area. Particle-supported structures tend to have a more uniform particle size distribution and retain more intergranular pores, while matrix-supported structures have an uneven distribution, with fine particles occupying storage space between coarse grains, resulting in high matrix microporosity content and strong stress sensitivity.

Fines content (*Fc*) is a more influential indicator to study the mechanical properties of binary particle media (Bell, 2013; Monkul et al., 2021; Zhou et al., 2018). *Fc* is defined as the ratio of sand and silt with $\emptyset > -2$ to gravel content of $-2 > \emptyset > -4$. Individual coarser gravels do not act as support for the pore space as elaborated in section 3.2 (Liu et al., 2022; Zhang et al., 2020b). The Young's modulus of the samples was calculated from the mineral fractions obtained from XRD experiments based on the VRH averaging theory (Digby, 1981). Samples with $Fc < 50\%$ are dominated by coarse intergranular contact, while samples with $Fc > 50\%$ exhibit a significant decrease in coarse intergranular contact and an increase in fine intergranular and coarse-fine contact (de Frias Lopez et al., 2016; Zhou et al., 2018). As shown in Fig. 9(d), samples transitioned from grain-supported to matrix-supported with increasing fines content. At the same time, Young's modulus decreases, making seepage channels more susceptible to compressive deformation and enhancing stress sensitivity.

Irreversible and reversible permeability damage rates were used to determine and quantify plastic and elastic deformation (Ruan and Wang, 2002; Cao and Lei, 2019). Fig. 9(c) shows a significant positive correlation ($R^2 > 0.8$) between stress sensitivity coefficient and plastic deformation amount, and a negative correlation with elastic deformation amount. Elastic deformation of hard coarse grains is small, while plastic deformation results from matrix particle deformation (body deformation) and rearrangement (structural deformation) (Cheng et al., 2023; Liu et al., 2020; Cao and Lei, 2019; Rahman Md and Lo, 2014). Particle unit structural deformation and pore filling by fine particles cause more significant and irreversible weakening of seepage channels, leading to stronger stress sensitivity.

According to experimental analysis, the stress sensitivity of sandy conglomerates in binary granular media is principally linked to the rock's supporting structure (matrix-supported and grain-supported), rock particles properties (radius *R*, Young's modulus *E*, and Poisson's ratio ν), and the pore radius *r*. The compressibility and support structure of the particles determine the pore percolation during compression. This provides a basis for establishing the quantitative characterization of stress sensitivity:

$$k(r, \sigma) = k(E, \nu, \sigma, R) \tag{8}$$

4.4. Particle compression model

The compressive deformation behavior of fine matrix particles is distinct from that of coarse grains. The matrix is more susceptible to plastic deformation, with matrix micropores and some dissolved pores being easily compressible, resulting in slit-like pores in the matrix-supported samples (Fig. 5(b)). Consequently, a four-particle model, capable of capturing structural deformation, is employed to describe the matrix behavior. On the other hand, coarse grains predominantly undergo elastic deformation of grains itself, and intergranular pores are less compressible and more spherical,

leading to the use of a three-particle model, focusing solely on bulk deformation.

4.4.1. Matrix compression model

The assumptions for the four-particle compression model of the matrix are as follows:

(1) Rock matrix pore consists of an accumulation of rock particles in a basic unit of four closely spaced particles, the particles in each unit being of equal diameter.
(2) Under external forces, the four-particle unit undergoes body and structural deformation. Body deformation involves elastic deformation, following Hertz's law of contact deformation with a circular contact surface of radius 'a'. Structural deformation occurs as the arrangement of the four particles varies, as shown in Fig. 10(c) and (d), transitioning from a square stack to a approaching rhomboidal stack.
(3) The fluid is a single-phase Newtonian fluid for single-phase flow. The relationship between fluid flow and pore radius follows Poiseuille's theory, and the relationship between permeability and flow is consistent with Darcy's law.
(4) The applied pressure is the external confining pressure on the particles; there's no alteration in pore pressure. The effective stress range aligns with experiment.

Hertz's law of contact deformation (Hertz, 1882) states that the radius a_m of the contact surface between rock particles subjected to external stress is given by

$$a_m = \sqrt[3]{\frac{3R_m F(1-\nu_m^2)}{4E_m}} \tag{9}$$

where R_m is the radius of the matrix particle, μm; F is the stress acting on the particle, N; ν_m is the Poisson's ratio of the matrix particle; and E_m is the Young's modulus of the matrix particle, Pa. The distance b_m from the particle center to the contact surface after deformation and the effective stress σ_m can be determined using this formula:

$$b_m = \sqrt{{R_m}^2 + {a_m}^2} \tag{10}$$

$$\sigma_m = \frac{2F}{\pi a_m^2} \tag{11}$$

After the effective stress increases, the granular units change from cubic to rhomboidal accumulation. The initial and changed cross-sectional areas of the pore seepage channels enclosed by the four particles A_{mo} and A'_m are

$$A_{mo} = (4-\pi)R_m^2 \tag{12}$$

$$A'_m = 4b_m^2 \sin\theta - \left(\pi - 4\arctan\frac{a_m}{b_m}\right)R_m^2 - 4a_m b_m \tag{13}$$

where θ is the inner angle of the rhombus formed by the line connecting the centers of the four particles. As the effective stress increases, θ decreases and the rate of decrease becomes smaller. The rate of decrease of θ is influenced by the friction between the particles, with a stronger frictional effect leading to a slower rate of deformation. The value of the friction between the two contact surfaces is proportional to the true contact area and the normal load (Bowden and Tabor, 2001; Lai et al., 2016). During deformation, the range of θ falls between $\pi/3$ and $\pi/2$. A function of the following form is constructed to describe the variation of θ:

$$\theta = \frac{\pi}{3} + \frac{\pi}{\left(\left(\sigma_m + \sqrt{6}\right)\left(\ln\left(1 + a_m^2/R_m\right) + \sqrt{6}\right)\right)^{\beta}} \tag{14}$$

When the effective stress is 0, the particles are in a square stacking state and the initial surface porosity enclosed by the four particles is denoted as n_{m0}. As the effective stress increases, the particles deform and their stacking state changes to a rhomboidal, and eventually to a positive rhomboidal. The resulting surface porosity is denoted as n'_m:

$$n_{m0} = 1 - \frac{\pi}{4} \approx 0.215 \tag{15}$$

$$n'_m = 1 - \frac{\left(\pi - 4\arctan\frac{a_m}{b_m}\right)R_m^2 + 4a_m b_m}{4b_m^2 \sin\theta} \tag{16}$$

4.4.2. Grain compression model

A model for compressive deformation of hard coarse grains using three-particle units is proposed, based on the following assumptions:

(1) Hard grains consist of three-particle structural units, the particles in each unit being of equal diameter, with small matrix particles filling the interior.
(2) Only body deformation occurs in the three-particle stacking unit under external force, following Hertz's law of contact deformation.
(3) The hard grains remain undeformed when squeezed against matrix. The pore seepage and pressure exertion law are the same as assumed in the previous section.

The circular radius a_p of the deformation zone and the distance b_p from the center of the particle to the contact surface after deformation are calculated using the same method as in Eqs. (9)

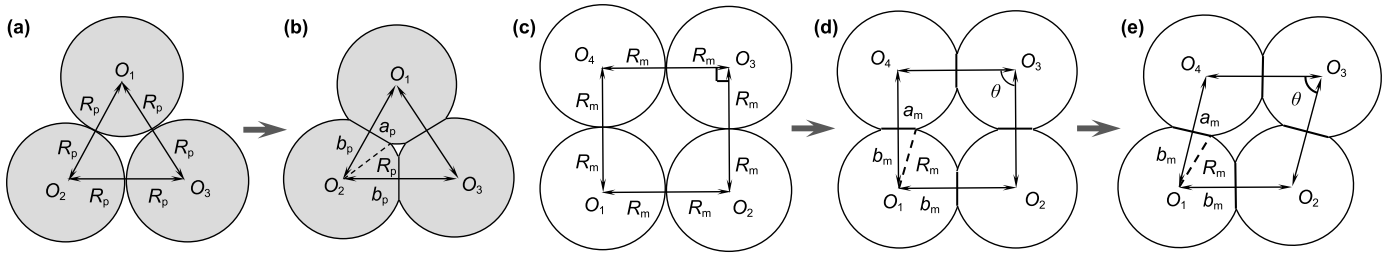

Fig. 10. Schematic diagram of the deformation of particles under pressure. **(a)**–**(b)** depict three-particle arrangements consisting of hard, coarse grains. **(c)**–**(e)** depict portray four-particle models representing fine matrix particles. While only body deformation occurs in **(b)** and **(d)**, both body and structural deformation occur in **(e)**.

and (10). The effective stress of the model is

$$\sigma_p = \frac{3F}{2\pi a_p^2} \tag{17}$$

The capillary cross-sectional areas A_{po} and A'_p before and after deformation of the particles are given by the following equations, respectively:

$$A_{po} = \left(\sqrt{3} - \pi \Big/ 2\right) R_p^2 \tag{18}$$

$$A'_p = \sqrt{3}b_p^2 - \frac{3}{2}\left(\frac{\pi}{3} - 2\arctan\frac{a_p}{b_p}\right)R_p^2 - 3a_p b_p \tag{19}$$

Thus, the surface porosity n_{p0} and n'_p in the initial state and after deformation are expressed in terms of the particle shape parameter as

$$n_{p0} = 1 - \frac{\sqrt{3}\pi}{6} \approx 0.093 \tag{20}$$

$$n'_p = 1 - \frac{\frac{3}{2}\left(\frac{\pi}{3} - 2\arctan\frac{a_p}{b_p}\right)R_p^2 + 3a_p b_p}{\sqrt{3}b_p^2} \tag{21}$$

4.5. Binary granular stress-sensitive model

4.5.1. Modelling and analysis

Fig. 11 shows that the pore space of the sandy conglomerate consists of two components: pores between the fine matrix particles and pores in the unoccupied spaces between coarse particles. Utilizing the mentioned assumptions, the undrained compression theory for binary granular accumulations can be referenced to formulate an overall porosity compression model (Chang et al., 2017b; Manzari and Dafalias, 2001). By applying Poiseuille theory and Darcy's law (Chapman and Palisch, 2014; Liu et al., 2020), the permeability ratios under different effective stress conditions effected by pore radius can be calculated:

$$n' = 1 - \delta(1 - n'_m) - \eta\left(1 - n'_p\right) \tag{22}$$

$$\frac{k'}{k_0} = \left[\frac{r'}{r_0}\right]^2 = \left[\frac{n'}{n_0}\right]^4 \tag{23}$$

where δ represents the deformation limitation factor of the matrix fines protected by the hard coarse grains supporting, with $\delta < 1$; η is the filling factor of the intergranular space between coarse grains by fines during compression, with $\eta > 1$. The calculation of parameters such as the particle size of binary particles for each sample is based on experimental data, which also helps to fully simulate the actual rock conditions. Fig. 12(a) shows the fitted results of the model and experimental data are accurate with $R^2 > 0.95$. Fig. 12(b) illustrates the relationship between the normalized permeability and the model parameters δ and η. The stress sensitivity of normalized permeability increases as δ and η increase. Specifically, an increase in the deformation limitation factor δ weakens the support capacity of coarse grains, leading to more structural deformation of fines units. Simultaneously, an increase in the particle rearrangement factor η promotes filling of the space between coarse particles by fine particles, resulting in

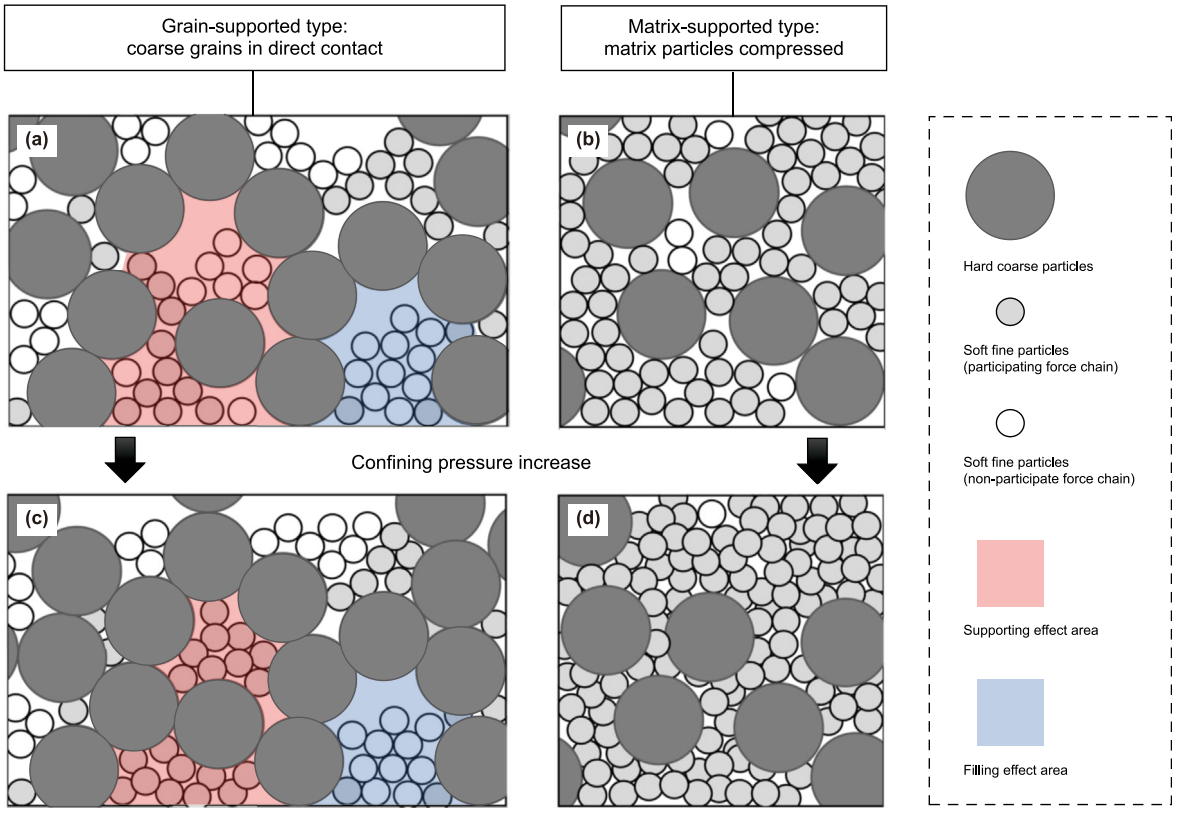

Fig. 11. Schematic diagram of a binary granular structure compressor. **(a)** and **(c)** depict the grain-supported type, where a support region and a filled region exist; **(b)** and **(d)** depict the matrix-supported type, where the matrix fine particles are directly compressed.

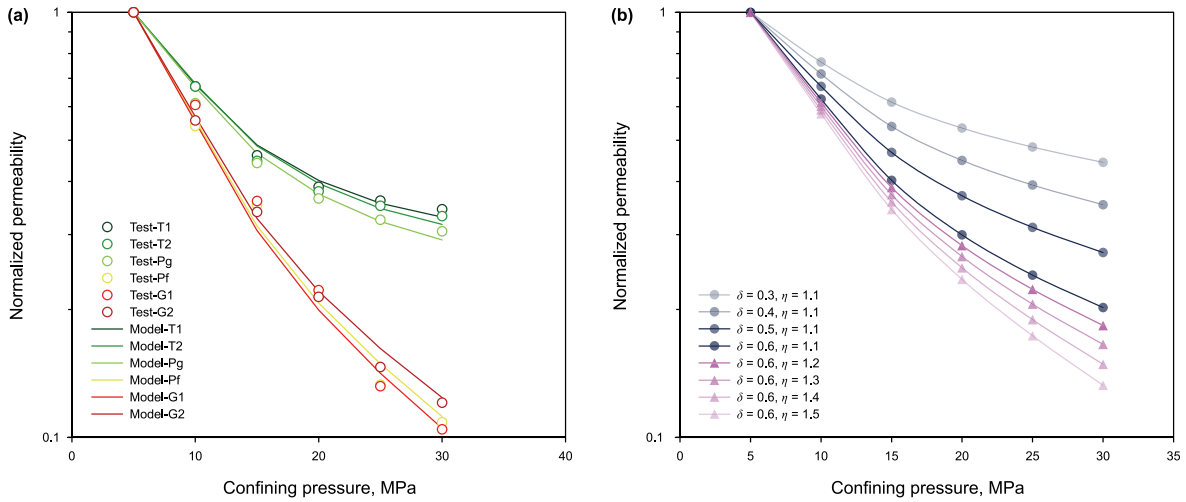

Fig. 12. **(a)** Comparison of preliminary model calculations with experimental data and **(b)** variation of normalized permeability with model parameters δ and η.

reduced surface porosity of the seepage channel and stronger stress sensitivity. Interestingly, both model parameters δ and η increase as the fines content of the sample increases, indicating that sandy conglomerate samples with a high fines content experience less support from hard coarse grains and more filling by fines.

The fitting results still have inaccuracies due to changing particle arrangement and nesting during compression, making deformation limitation factor and filling factor non-constant (Rahman Md and Lo, 2014). It is necessary to introduce the concept of force chains to describe the non-steady state of the compression process (Casagrande, 1976). Another equivalent formulation of this state is that, for a given porosity, there is no unique chain of forces that deforms the particle structure continuously. Specifically, for binary granular structures with different sizes and compression properties, some of the fine particles are obscured in the voids of the coarse particles and do not actively participate in the transfer of normal forces. Changes in effective stress alter active contents of fine particles in force chains, affecting particle's support and filling capacity. This impacts rock compliance and resistance to sliding and failure. To capture the dynamic effects of force chains, the proportion changes of fine particles playing an active role in the force chain must be considered. This proportion can be expressed in exponential form with respect to effective stress (Zhou et al., 2018). Therefore, following the approach of Thevanayagam et al. (Chang and Yin, 2011; Thevanayagam, 1998; Zhou et al., 2018), we improved the model presented in the previous section:

$$n' = 1 - \left(1 + Fc - n'_{\mathrm{m}}Fc - n'_{\mathrm{p}}\right)c' \tag{24}$$

$$c' = c^{(\sigma/\sigma_0)} \tag{25}$$

where Fc denotes the fines content in the sample. Model parameter c known as force chain flexibility, determines the trends of change of active content of fine particles in force chains as effective stress increases and reflects the rearrangement ability of binary particles. $c = 1$ corresponds to the steady state of the unary granular system, $c < 1$ indicates the gradual dominance of hard grains, and $c > 1$ implies that more fine particles fill the pores between the hard grains and participate in the force chain transfer. Eqs. (24) and (25) accurately fit experimental results, with $R^2 > 0.97$, as shown in Fig. 13(a).

Fig. 13(b) depicts how the ratio of the active content of fine particles relative to the initial active content varies with the effective stress in each sample. It is evident that for the grains-supported samples (T1, T2, Pg), the active content of fine particles decreases with increasing effective stress, leading to the formation of a stable structure of coarse particles supported by each other. For the matrix-supported samples, more and more fine particles play an active role in the force chains, indicating the predominance of the filling role of fine particles. The study shows that there is a small number of fine particles that are not in an active state at the initial moment of the binary particulate media involved in this study (Chang and Yin, 2011; Zhou et al., 2018), and it is the number of particles that provides the scope for the variation in the fine particles active content. However, the c of the sample with the highest fine particle content (Pf sample) is smaller than that of the G samples due to the reduced mutual contact between the coarse particles when the fine particle content is too high. In this case, the compression process is closer to that of a single-particles rock sample, with c converging to 1. This conclusion is consistent with the findings of Liu et al. (2022), who reported a decrease in interconnection when the coarse grains content < 35%. Thus, as shown in Fig. 14, the stress-sensitive of binary granular samples, such as sandy conglomerates, can be classified into three types: support-dominated, fill-dominated, and matrix-controlled, using $c = 1$ and $Fc = 65\%$ as critical values.

4.5.2. Application of the model

The Mahu conglomerate reservoir, situated in Xinjiang, China, is known to harbors typical binary granular media reservoirs. The presence of stress sensitivity can cause a significant decrease in production capacity. Therefore, it is of utmost importance to maintain a reasonable bottomhole pressure to mitigate such losses. As an example, the parameters of an actual well are considered. With a formation pressure P_{e} of 61.8 MPa, a drainage radius r_{e} of 240 m, a reservoir thickness h of 20 m, and a starting pressure gradient λ of 0.01 MPa/m, the radial flow rate v can be expressed as

$$v = \frac{K_0 \mathrm{e}^{-\gamma(P_{\mathrm{e}}-P)}}{\mu}\left(\frac{\mathrm{d}p}{\mathrm{d}r} - \lambda\right) \tag{26}$$

The equation for radial flow production energy considering stress-sensitive effects is established by expanding and integrating the above equation:

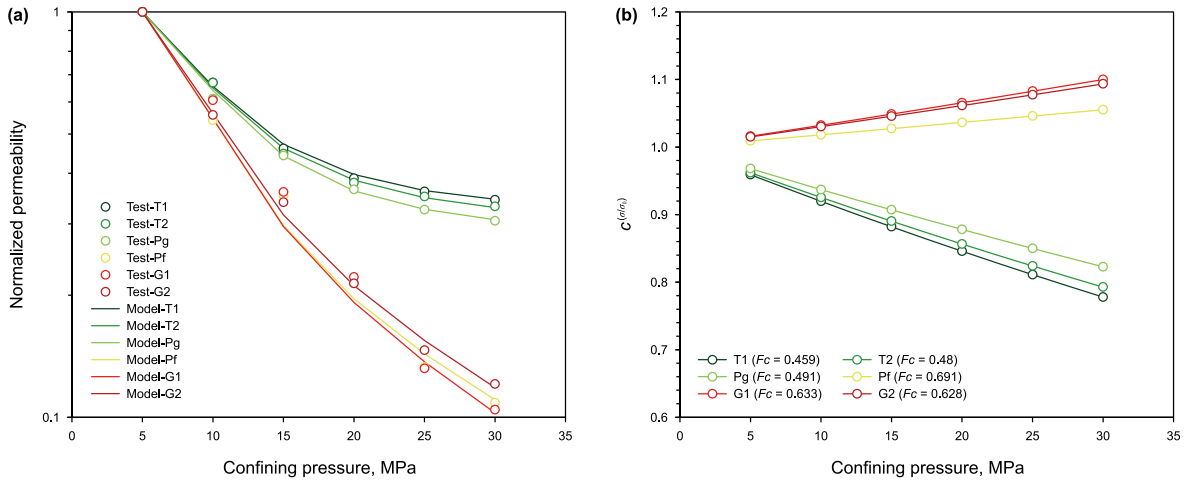

Fig. 13. **(a)** Comparison of the improved model with experimental data. **(b)** Variation of the ratio of the active content of fine particles relative to the initial active content with increasing effective stress for six samples.

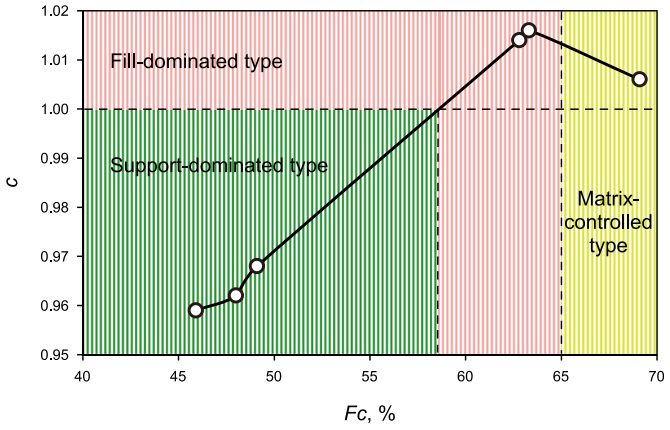

Fig. 14. Stress-sensitive types according to force chain flexibility *c* and fines content *Fc*. The green area indicates the support-dominated type; the red area indicates the fill-dominated type; the yellow area indicates the matrix-controlled type.

$$Q = \frac{2\pi h K_0 \left\{ \left[1 - e^{-\gamma(P_e - P_w)} \right] - \gamma\lambda e^{-\gamma(P_e - \overline{P})} (r_e - r_w) \right\}}{\gamma \mu B_o \ln\left(\frac{r_e}{r_w}\right)} \tag{27}$$

where P_w is the bottomhole pressure, MPa; P is the pressure at a point in the plane, MPa; $\overline{P}$ is the average reservoir pressure, MPa; r_w is the well radius, m; μ is the fluid viscosity, mPa·s; and B_o is the fluid volume factor. Based on the model in this study, an exponential relationship between permeability and effective stress for a given reservoir can be obtained. The formations data meeting the selected boundary values in Fig. 14 were used to calculate the predicted production with and without stress sensitivity at different wellbore pressures. As depicted in Fig. 15, the production retention rate increases with an increase in bottomhole pressure, indicating that increasing the bottomhole pressure can help reduce the stress-sensitive damage. To limit the stress-sensitive damage to production to 20%, it is recommended that for tight reservoirs of the support-dominated type (Group A samples in this study), the wellbore pressure should be higher than 43.35 MPa, i.e., the energy retention rate should be greater than 70.1%. For fill-dominated type and matrix-controlled tight reservoirs (Group B samples in this

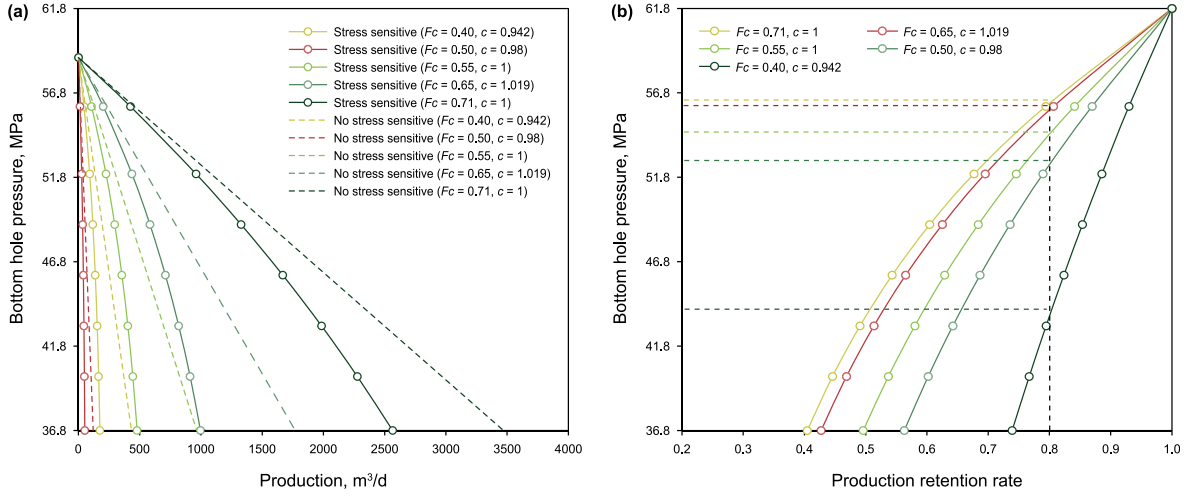

Fig. 15. **(a)** Comparison of production with and without stress sensitivity at different bottom hole pressures. **(b)** Production retention at different bottom hole pressures.

study), the bottomhole pressure should be higher than 54.4 and 55.8 MPa, respectively, i.e., the energy retention rate should be higher than 88% and 90.2%.

5. Conclusion

In this study, we investigated the stress-sensitive mechanism of compact sand conglomerates, and the key findings are as follows:

(1) The stress-sensitivity coefficients for tight sandy conglomerates ranged from 65.6% to 90.9%, with permeability damage rates from 65.6% to 90.9%, and an average pore compression coefficient between 0.0168 and 0.0208 MPa^{-1}. Pore compressibility decreased with increasing stress and can be divided into three stages: filling, compression, and compaction. Pore compression was mainly controlled by matrix pores.

(2) The stress sensitivity of binary granular media is influenced by the support structure and granular properties. Matrix-supported samples exhibited high stress sensitivity coefficients (average = 0.089) and irreversible permeability damage rates (average = 74.2%). In contrast, grain-supported samples showed very low late stress sensitivity coefficients (average = 0.021) for effective stress >15 MPa. The stress sensitivity of binary particulate media with small fine particle size, high fines content, high uniformity coefficient of particle size, high matrix pore content, high plastic deformation, and low Young's modulus was found to be high.

(3) Based on the Hertz contact deformation theory and Poiseuille theory, we derived semi-analytical models of three-particle and four-particle compression for hard grains and matrix particles. We further considered the support and filling effects of binary particles to establish a nested stress-sensitive model, with a calculation error <0.05.

(4) By considering the change of the active content of fine particles in the force chain during stress action, we developed an improved model for the non-stationary characteristics of stress sensitivity, with an average error <0.03. Binary granular media were classified into three types based on the model parameters: support-dominated, filling-dominated, and matrix-controlled. Applying the model to China's Mahu reservoir, the formation energy retention rates for these three types of reservoirs were found to be at least 70.1%, 88%, and 90.2%, respectively, while ensuring that production stress sensitivity loss remains below 20%.

Declaration of competing interest

The authors declare that they have no known competing financial interests or personal relationships that could have appeared to influence the work reported in this paper.

CRediT authorship contribution statement

Jian-Bang Wu: Conceptualization, Investigation, Methodology, Software, Visualization, Writing – original draft, Writing – review & editing. **Sheng-Lai Yang:** Conceptualization, Project administration, Writing – review & editing. **Qiang Li:** Data curation, Software. **Kun Yang:** Resources, Validation. **Can Huang:** Methodology. **Dao-Ping Lv:** Conceptualization, Funding acquisition, Project

Appendix A. Nomenclature

T_2, T_{2s}	Transverse relaxation of NMR, surface relaxation of NMR, ms	σ_m, σ_p	Effective stress of matrix particle, effective stress of coarse grain, Pa
ρ	Constant that represents the relaxation strength	A_{mo}, A'_m, A_{po}, A'_p	Initial and changed cross-sectional areas of the pore seepage channels enclosed by matrix particles or coarse grains, respectively, m^2
D	Permeability damage rate corresponding to the pressure, %	θ	Inner angle of the rhombus formed by the line connecting the centers of the four particles
k, K_0, K	Permeability, initial permeability, permeability under the corresponding effective stress, mD	n_{mo}, n'_m, n_{po}, n'_p	Initial and changed surface porosity enclosed by matrix particles or coarse grains, respectively
γ	Stress sensitivity coefficient	β	Model parameter
σ, σ_0, σ_i	Effective stress, initial effective stress, a certain effective stress, MPa	n_0, n'	Initial overall surface porosity, overall surface porosity under the corresponding effective stress
C_P	Pore volume compressibility coefficient, MPa^{-1}	δ	Deformation limitation factor of the matrix fines
S_0, S_i	Initial T_2 spectrum envelope area, T_2 spectrum envelope area under the corresponding effective stress	η	Filling factor of the matrix fines
ϕ/ϕ_0	Ratio of the porosity corresponding to the effective stress relative to the initial porosity	Fc	Fines content, %
A	Power exponent of porosity-permeability	c, c'	Force chain flexibility, active content of fine particles in force chains
D_p	Particle diameter, mm	E_p	Stage compression ratio
Ø	Logarithm of the particle diameter on a base of 2	ζ	Comparison coefficients of stage compression ratio for macropores and micropores
r, r_0, r'	Pore radius, initial pore radius, pore radius under the corresponding effective stress, m	h	Reservoir thickness, m
E, E_m, E_p	Young's modulus, Young's modulus of matrix particle, Young's modulus of coarse grain, Pa	r_e, r_w	Drainage radius, well radius, m
ν, ν_m, ν_p	Poisson's ratio, poisson's ratio of matrix particle, poisson's ratio of coarse grain	P_e, P_w, $P, \overline{P}$	Formation pressure, bottomhole pressure, pressure at a point in the plane, average reservoir pressure, MPa
R, R_m, R_p	Particle radius, matrix particle radius, coarse grain radius, μ m	λ	Starting pressure gradient, MPa/m
a_m, a_p	Radius of the contact surface between rock particles subjected to external stress, for matrix particle and coarse grain, respectively, m	M	Fluid viscosity, mPa·s,
b_m, b_p	Distance from the center of the particle to the contact surface after deformation, for matrix particle and coarse grain, respectively, m	B_o	Fluid volume factor
F	Stress acting on the particle, N	P_P	Pore pressure, MPa

administration. **Wei Zhou:** Funding acquisition.

Acknowledgements

This research was funded in part by the National Natural Science Foundation of China, grant number 51574257, in part by the National Key Research and Development Program of China, grant number 2015CB250904.

References

Bell, F.G., 2013. Engineering Properties of Soils and Rocks. Elsevier.
Bernabé, Y., Mok, U., Evans, B., 2003. Permeability-porosity relationships in rocks subjected to various evolution processes. Pure Appl. Geophys. 160, 937–960. https://doi.org/10.1007/PL00012574.
Bowden, F.P., Tabor, D., 2001. The Friction and Lubrication of Solids. Oxford university press.
Cao, N., Lei, G., 2019. Stress sensitivity of tight reservoirs during pressure loading and unloading process. Petrol. Explor. Dev. 46, 138–144. https://doi.org/10.1016/S1876-3804(19)30013-8.
Casagrande, A., 1976. Liquefaction and Cyclic Deformation of Sands: A Critical Review, 19791976.
Chang, C.S., Yin, Z.-Y., 2011. Micromechanical modeling for behavior of silty sand with influence of fine content. Int. J. Solids Struct. 48, 2655–2667. https://doi.org/10.1016/j.ijsolstr.2011.05.014.
Chang, C.S., Deng, Y., Yang, Z., 2017a. Modeling of minimum void ratio for granular soil with effect of particle size distribution. J. Eng. Mech. 143, 04017060. https://doi.org/10.1061/(ASCE)EM.1943-7889.0001270.
Chang, C.S., Meidani, M., Deng, Y., 2017b. A compression model for sand–silt mixtures based on the concept of active and inactive voids. Acta Geotech 12, 1301–1317. https://doi.org/10.1007/s11440-017-0598-1.
Chapman, M., Palisch, T., 2014. Fracture conductivity—Design considerations and benefits in unconventional reservoirs. J. Petrol. Sci. Eng. 124, 407–415. https://doi.org/10.1016/j.petrol.2014.09.015.
Chen, D., Pan, Z., Ye, Z., 2015. Dependence of gas shale fracture permeability on effective stress and reservoir pressure: model match and insights. Fuel 139, 383–392. https://doi.org/10.1016/j.fuel.2014.09.018.
Chen, Z., Fu, L., Zhou, C., et al., 2022. Analysis of factors affecting the reservoir quality of deepwater gravity flow tight sandstone: a case study of the Chang 6 oil reservoir of the Yanchang Formation in the Huaqing area, China. Arabian J. Geosci. 15 (229). https://doi.org/10.1007/s12517-021-09321-3.
Chen, T.-Y., Hao, Y.-Y., Elsworth, D., et al., 2023. Modes of multi-mechanistic gas diffusion in shale matrix at varied effective stresses: observations and analysis. Petrol. Sci. https://doi.org/10.1016/j.petsci.2023.03.016.
Cheng, K., Wu, H., Fang, Y., et al., 2023. Experimental study on shear wave velocity of sand-gravel mixtures considering the effect of gravel content. Front. Earth Sc-Switz 10. https://doi.org/10.3389/feart.2022.1076098.
Crawford, B., Cronin, M., Ijasan, O., et al., 2023. Poroelastic prediction of matrix compressibility and pressure dependent permeability: impact on simulated recovery factors in permian basin resource rocks. In: USA, SPE/AAPG/SEG Unconventional Resources Technology Conference. URTEC, D031S060R003. https://doi.org/10.15530/urtec-2023-3856929.
David, C., Wong, T.-F., Zhu, W., et al., 1994. Laboratory measurement of compaction-induced permeability change in porous rocks: implications for the generation and maintenance of pore pressure excess in the crust. Pure Appl. Geophys. 143, 425–456. https://doi.org/10.1007/BF00874337.
de Frias Lopez, R., Silfwerbrand, J., Jelagin, D., et al., 2016. Force transmission and soil fabric of binary granular mixtures. Géotechnique 66, 578–583. https://doi.org/10.1680/jgeot.14.P.199.
Digby, P.J., 1981. The effective elastic moduli of porous granular rocks. J. Appl. Mech. 48, 803–808. https://doi.org/10.1115/1.3157738.
Dormieux, L., Jeannin, L., Gland, N., 2011. Homogenized models of stress-sensitive reservoir rocks. Int. J. Eng. Sci. 49, 386–396. https://doi.org/10.1016/j.ijengsci.2010.12.010.
Faruk, C., 2000. Predictability of porosity and permeability alterations by geochemical and geomechanical rock and fluid interactions. In: SPE International Symposium on Formation Damage Control. https://doi.org/10.2118/58746-MS.
Fatt, I., Davis, D., 1952. Reduction in permeability with overburden pressure. J. Petrol. Technol. 4, 16. https://doi.org/10.2118/952329-G.
Gangi, A.F., 1978. Variation of whole and fractured porous rock permeability with confining pressure. Int. J. Rock Mech. Min. 15, 249–257. https://doi.org/10.1016/0148-9062(78)90957-9.
Gao, H., Wang, C., Cao, J., et al., 2019. Quantitative study on the stress sensitivity of pores in tight sandstone reservoirs of Ordos Basin using NMR technique. J. Petrol. Sci. Eng. 172, 401–410. https://doi.org/10.1016/j.petrol.2018.09.083.
Gao, W., Li, Y., Kong, D., et al., 2023. Effect of grain size distribution on pore size distribution characteristics in a conglomerate reservoir from an alluvial fan via artificial rock approach. SPE J. 28 (6), 3063–3078. https://doi.org/10.2118/217426-PA.
Gu, Y., Ding, W., Yin, M., et al., 2018. Study on pressure sensitivity of tight sandstone and its influence on reservoir characteristics. Energy Sources, Part A Recovery, Util. Environ. Eff. 40, 2671–2677. https://doi.org/10.1080/15567036.2018.1503753.
Guéguen, Y., Boutéca, M., 2004. Mechanics of Fluid-Saturated Rocks. Elsevier, 9780080479361.
Guéguen, Y., Fortin, J., 2013. Elastic envelopes of porous sandstones. Geophys. Res. Lett. 40, 3550–3555. https://doi.org/10.1002/grl.50676.
Gupta, I., Rai, C., Sondergeld, C., 2019. Study impact of sample treatment and insitu fluids on shale wettability measurement using NMR. J. Petrol. Sci. Eng. 176, 352–361. https://doi.org/10.1016/j.petrol.2019.01.048.
Han, J., Wu, C., Jiang, X., et al., 2022. Investigation on effective stress coefficients and stress sensitivity of different water-saturated coals using the response surface method. Fuel 316, 123238. https://doi.org/10.1016/j.fuel.2022.123238.
He, J., Guo, X., Cui, H., et al., 2022. Stress sensitivity of tight sand reservoir and its influence on productivity of well. Petrol. Sci. Technol. 40, 1665–1680. https://doi.org/10.1080/10916466.2022.2026960.
Hertz, H., 1882. On the Contact of Rigid Elastic Solids and on Hardness (chapter 6): Assorted papers by H. Hertz.
Holt, R.M., Bakk, A., Fjær, E., et al., 2005. Stress sensitivity of wave velocities in shale. SEG Technical Program Expanded Abstracts, pp. 1593–1596.
Ivars, D.M., Pierce, M.E., Darcel, C., et al., 2011. The synthetic rock mass approach for jointed rock mass modelling. Int. J. Rock Mech. Min. 48, 219–244. https://doi.org/10.1016/j.ijrmms.2010.11.014.
Kang, W.-L., Zhou, B.-B., Issakhov, M., Gabdullin, M., 2022. Advances in enhanced oil recovery technologies for low permeability reservoirs. Petrol. Sci. 19, 1622–1640. https://doi.org/10.1016/j.petsci.2022.06.010.
Krumbein, W.C., 1934. Size frequency distributions of sediments. J. Sediment. Res. 4, 65–77. https://doi.org/10.1306/D4268EB9-2B26-11D7-8648000102C1865D.
Lai, T., Zhu, S., Huang, P., 2016. Adhesion behavior of a grating at a single location by using an AFM flat tip under different conditions. J. Adhes. 92, 194–213. https://doi.org/10.1080/00218464.2015.1018512.
Li, S., Tang, D.Z., Pan, Z.J., et al., 2013. Characterization of the stress sensitivity of pores for different rank coals by nuclear magnetic resonance. Fuel 111, 746–754. https://doi.org/10.1016/j.fuel.2013.05.003.
Li, J.-H., Li, B.-B., Cheng, Q.-Y., et al., 2022a. Characterization of the fracture compressibility and its permeability for shale under the effects of proppant embedment and compaction: a preliminary study. Petrol. Sci. 19, 1125–1138. https://doi.org/10.1016/j.petsci.2021.12.021.
Li, Y., Chen, J.-Q., Yang, J.-H., et al., 2022b. Determination of shale macroscale modulus based on microscale measurement: a case study concerning multi-scale mechanical characteristics. Petrol. Sci. 19, 1262–1275. https://doi.org/10.1016/j.petsci.2021.10.004.
Li, X., Duan, K., Zhang, Q., et al., 2023. Investigation of the permeability anisotropy of porous sandstone induced by complex stress conditions. Comput. Geotech. 157, 105309. https://doi.org/10.1016/j.compgeo.2023.105309.
Liu, K., Yin, D., Sun, Y., 2020. The mathematical model of stress sensitivities on tight reservoirs of different sedimentary rocks and its application. J. Petrol. Sci. Eng. 193, 107372. https://doi.org/10.1016/j.petrol.2020.107372.
Liu, B., Yang, Y., Li, J., et al., 2020. Stress sensitivity of tight reservoirs and its effect on oil saturation: a case study of Lower Cretaceous tight clastic reservoirs in the Hailar Basin, Northeast China. J. Petrol. Sci. Eng. 184, 106484. https://doi.org/10.1016/j.petrol.2019.106484.
Liu, J., Ge, H., Zhang, Z., et al., 2022. Influence of mechanical contrast between the matrix and gravel on fracture propagation of glutenite. J. Petrol. Sci. Eng. 208, 109639. https://doi.org/10.1016/j.petrol.2021.109639.
Manzari, M., Dafalias, Y., 2001. A Critical State Bounding Surface Model for Sands, pp. 1164–1170.
McLatchie, A., Hemstock, R., Young, J., 1958. The effective compressibility of reservoir rock and its effects on permeability. J. Petrol. Technol. 10, 49–51. https://doi.org/10.2118/894-G.
Mitchell, J.K., Soga, K., 2005. Fundamentals of Soil Behavior, vol. 3. John Wiley & Sons, New York, 978-0-471-46302-3.
Monkul, M.M., Kendir, S.B., Tütüncü, Y.E., 2021. Combined effect of fines content and uniformity coefficient on cyclic liquefaction resistance of silty sands. Soil Dynam. Earthq. Eng. 151, 106999. https://doi.org/10.1016/j.soildyn.2021.106999.
Núñez-González, F., Martín-Vide, J.P., Kleinhans, M.G., 2016. Porosity and size gradation of saturated gravel with percolated fines. Sedimentology 63, 1209–1232. https://doi.org/10.1111/sed.12257.
Petunin, V.V., Yin, X., Tutuncu, A.N., 2011. Porosity and permeability changes in sandstones and carbonates under stress and their correlation to rock texture. In: Canadian Unconventional Resources Conference. https://doi.org/10.2118/147401-MS.
Raghavan, R., Chin, L.Y., 2002. Productivity changes in reservoirs with stress-dependent permeability. In: SPE Annual Technical Conference and Exhibition. https://doi.org/10.2118/77535-MS.
Rahman Md, M., Lo, S.R., 2014. Undrained behavior of sand-fines mixtures and their state parameter. J. Geotech. Geoenviron. 140, 04014036. https://doi.org/10.1061/(ASCE)GT.1943-5606.0001115.
Ruan, M., Wang, L., 2002. Low-permeability oilfield development and pressure-sensitive effect. Acta Pet. Sin. 23 (73). https://doi.org/10.7623/syxb200203016.
Sayers, C.M., 2023. The effect of clay and contacts between sand grains on the

elastic properties of sandstones. Geophys. Prospect. 71, 456–470. https://doi.org/10.1111/1365-2478.13318.
Shi, X., Wang, M., Wang, Z., et al., 2021. A brittleness index evaluation method for weak-brittle rock by acoustic emission technique. J. Nat. Gas Sci. Eng. 95, 104160. https://doi.org/10.1016/j.jngse.2021.104160.
Sonmez, H., Gokceoglu, C., Medley, E.W., et al., 2006. Estimating the uniaxial compressive strength of a volcanic bimrock. Int. J. Rock Mech. Min. 43, 554–561. https://doi.org/10.1016/j.ijrmms.2005.09.014.
Tai, P.L., Dong, J.J., 2022. The influence of confining stress and pore pressure on effective stress coefficient for permeability: a novel Discretized Clay Shell Model for clayey sandstone. J. Nat. Gas Sci. Eng. 106, 104777. https://doi.org/10.1016/j.jngse.2022.104777.
Terzaghi, K., Peck, R.B., 1948. Soil Mechanics. Engineering Practice. John Wiley and Sons, Inc., New York.
Thevanayagam, S., 1998. Effect of fines and confining stress on undrained shear strength of silty sands. J. Geotech. & Geoenviron. 124, 479–491. https://doi.org/10.1061/(ASCE)1090-0241(1998)124:6(479).
Thevanayagam, S., 2000. Liquefaction potential and undrained fragility of silty soils. In: Proceedings of the 12th World Conference Earthquake.
Thevanayagam, S., Shenthan, T., Mohan, S., et al., 2002. Undrained fragility of clean sands, silty sands, and sandy silts. J. Geotech. Geoenviron. 128, 849–859. https://doi.org/10.1061/(ASCE)1090-0241(2002)128:10(849).
Tian, X., Cheng, L., Cao, R., et al., 2015. A new approach to calculate permeability stress sensitivity in tight sandstone oil reservoirs considering micro-pore-throat structure. J. Petrol. Sci. Eng. 133, 576–588. https://doi.org/10.1016/j.petrol.2015.05.026.
Tian, W., Lu, S., Zhang, J., et al., 2022. NMR characterization of fluid mobility in low-permeability conglomerates: an experimental investigation of spontaneous imbibition and flooding. J. Petrol. Sci. Eng. 214, 110483. https://doi.org/10.1016/j.petrol.2022.110483.
Wang, Z., Wang, R., Li, T., et al., 2017. The combined effects of pore structure and pore fluid on the acoustic properties of cracked and vuggy synthetic rocks. J. Petrol. Sci. Eng. 156, 202–211. https://doi.org/10.1016/j.petrol.2017.05.023.
Wang, H., Oyenowo, O.P., Okuno, R., 2023. Aqueous formate solution for enhanced water imbibition in oil recovery and carbon storage in carbonate reservoirs. Fuel 345, 128198. https://doi.org/10.1016/j.fuel.2023.128198.
Xiao, W., Li, T., Li, M., et al., 2016. Evaluation of the stress sensitivity in tight reservoirs. Petrol. Explor. Dev. 43, 115–123. https://doi.org/10.1016/S1876-3804(16)30013-1.
Xiao, Q.H., Zhao, X.L., Lin, W., et al., 2019. Application of NMR to test sandstone stress sensitivity of the Dongfang X Gas Field, China. IEEE Access 7, 95212–95223. https://doi.org/10.1109/ACCESS.2019.2928567.
Xu, C., Lin, C., Kang, Y., et al., 2018. An experimental study on porosity and permeability stress-sensitive behavior of sandstone under hydrostatic compression: characteristics, mechanisms and controlling factors. Rock Mech. Rock Eng. 51, 2321–2338. https://doi.org/10.1007/s00603-018-1481-6.
Xu, Y., Xiao, J., Li, X., et al., 2023. Experimental study on the permeability evolution of argillaceous sandstone under elevated temperatures. Eng. Geol. 313, 106974. https://doi.org/10.1016/j.enggeo.2022.106974.
Yang, W., Hou, J., Liu, Y., et al., 2022. The pore structures of different lithofacies in low-permeability sandy conglomerate reservoirs and their diagenetic impacts: a case study from the Es_4 member of the northern steep slope in Dongying Depression, Bohai Bay Basin, NE China. Mar. Petrol. Geol. 136, 105481. https://doi.org/10.1016/j.marpetgeo.2021.105481.
Zhang, C., Song, X., Wang, X., et al., 2014. A novel quantitative petrophysical model for the stress sensitivity of tight sandstones. J. Petrol. Sci. Eng. 122, 657–666. https://doi.org/10.1016/j.petrol.2014.09.008.
Zhang, R., Ning, Z., Yang, F., et al., 2016. A laboratory study of the porosity-permeability relationships of shale and sandstone under effective stress. Int. J. Rock Mech. Min. 81, 19–27. https://doi.org/10.1016/j.ijrmms.2015.11.006.
Zhang, J.J., Wei, C.T., Ju, W., et al., 2019. Stress sensitivity characterization and heterogeneous variation of the pore-fracture system in middle-high rank coals reservoir based on NMR experiments. Fuel 238, 331–344. https://doi.org/10.1016/j.fuel.2018.10.127.
Zhang, C., Song, X., Wang, X., et al., 2020a. Origin and depositional characteristics of supported conglomerates. Petrol. Explor. Dev. 47, 292–305. https://doi.org/10.1016/s1876-3804(20)60047-7.
Zhang, K., Wu, S., Zhong, Y., et al., 2020b. Modal distribution of pore-throat size in sandy conglomerates from an alluvial fan environment: lower Karamay Formation, Junggar Basin, West China. Mar. Petrol. Geol. 117, 104391. https://doi.org/10.1016/j.marpetgeo.2020.104391.
Zhang, K., Wu, S.H., Zhong, Y.C., et al., 2020c. Modal distribution of pore-throat size in sandy conglomerates from an alluvial fan environment: lower Karamay Formation, Junggar Basin, West China. Mar. Petrol. Geol. 117. https://doi.org/10.1016/j.marpetgeo.2020.104391.
Zhang, W., Huang, Z., Guo, X., et al., 2020d. A study on pore systems of Silurian highly mature marine shale in Southern Sichuan Basin, China. J. Nat. Gas Sci. Eng. 76, 103094. https://doi.org/10.1016/j.jngse.2019.103094.
Zhang, T., Ming, T., Yuan, L., et al., 2023. Experimental study on stress-dependent multiphase flow in ultra-low permeability sandstone during CO_2 flooding based on LF-NMR. Energy 278, 127874. https://doi.org/10.1016/j.energy.2023.127874.
Zhao, L., Chen, Y., Ning, Z., et al., 2013. Stress sensitive experiments for abnormal overpressure carbonate reservoirs: a case from the Kenkiyak fractured-porous oil field in the littoral Caspian Basin. Petrol. Explor. Dev. 40, 208–215. https://doi.org/10.1016/S1876-3804(13)60024-5.
Zhao, N., Wang, L., Sima, L., et al., 2022. Understanding stress-sensitive behavior of pore structure in tight sandstone reservoirs under cyclic compression using mineral, morphology, and stress analyses. J. Petrol. Sci. Eng. 218, 110987. https://doi.org/10.1016/j.petrol.2022.110987.
Zhong, X., Zhu, Y., Liu, L., et al., 2020a. The characteristics and influencing factors of permeability stress sensitivity of tight sandstone reservoirs. J. Petrol. Sci. Eng. 191, 107221. https://doi.org/10.1016/j.petrol.2020.107221.
Zhong, X.Y., Zhu, Y.S., Liu, L.P., et al., 2020b. The characteristics and influencing factors of permeability stress sensitivity of tight sandstone reservoirs. J. Petrol. Sci. Eng. 191. https://doi.org/10.1016/j.petrol.2020.107221.
Zhou, W., Wu, W., Ma, G., et al., 2018. Undrained behavior of binary granular mixtures with different fines contents. Powder Technol. 340, 139–153. https://doi.org/10.1016/j.powtec.2018.09.022.